

Evolutionary tradeoff and equilibrium in an aquatic predator-prey system

Laura E. Jones*
Stephen P. Ellner†

November 13, 2018

CORNELL UNIVERSITY
Department of Ecology and Evolutionary Biology
E145 Corson Hall
Ithaca, New York 14853-2701

*lej4@cornell.edu

†spe2@cornell.edu

Abstract

Due to the conventional distinction between *ecological* (rapid) and *evolutionary* (slow) timescales, ecological and population models to date have typically ignored the effects of evolution. Yet the *potential* for rapid evolutionary change has been recently established and may be critical to understanding how populations adapt to changing environments. In this paper we examine the relationship between ecological and evolutionary dynamics, focusing on a well-studied experimental aquatic predator-prey system (Fussmann et al. 2000; Shertzer et al. 2002; Yoshida et al. 2003). Major properties of predator-prey cycles in this system are determined by ongoing evolutionary dynamics in the prey population. Under some conditions, however, the populations tend to apparently stable steady-state densities. These are the subject of the present paper. We examine a previously developed model for the system, to determine how evolution shapes properties of the equilibria, in particular the number and identity of coexisting prey genotypes. We then apply these results to explore how evolutionary dynamics can shape the responses of the system to “management”: externally imposed alterations in conditions. Specifically, we compare the behavior of the system including evolutionary dynamics, with predictions that would be made if the potential for rapid evolutionary change is neglected. Finally, we posit some simple experiments to verify our prediction that evolution can have significant qualitative effects on observed population-level responses to changing conditions.

1 Introduction

A distinction is often made between *ecological* and *evolutionary* time scales, the former referring to relatively rapid changes in the distribution and abundance of species, the latter to more gradual changes in the properties of those species as a result of natural selection. This distinction is tacitly embedded in much of the established theory in ecology and evolution. Ecological models conventionally assume constant parameters to characterize species and their interactions (a recent influential text on community ecology (Morin 1999) does not even list evolution among the “factors influencing interactions among species”). Conversely, many evolutionary and population-genetic models assume constant population size on the grounds that (relative to the evolutionary time scale) ongoing changes in population size are merely high-frequency “noise”. When population dynamics are considered, only rare extreme events (bottlenecks, expansion after colonization, etc.) are assumed to matter. Even in theories that explicitly combine ecological and evolutionary dynamics, the separation of time-scales is typically assumed. For example, Khibnik and Kondrashov (1997) analyze predator-prey coevolution using singular perturbation theory, assuming that ecological dynamics are much faster than evolution. The “canonical equation” of Adaptive Dynamics (Marrow et al. 1996, Dieckmann et al. 1997) used in many recent papers (e.g. Dercole

et al. 2003, Le Galliard et al. 2003) goes even further, and assumes evolutionary changes are so rare that ecological dynamics reach their new asymptotic steady-state or attractor before another evolutionary step occurs.

However, recent years have seen an accumulation of evidence that this presumed separation of time scales is often violated (e.g., Thompson 1998, Hairston et al. 1999, Cousyn et al. 2001, Reznick and Ghalambor 2001, Grant and Grant 2002, Yoshida et al. 2003): in natural and experimental settings, trait evolution and changes in abundance may occur on similar time scales. For example, Resnick et al. (1997) observed significant life history evolution in guppies over periods of 4-11 years in response to changes in predation pressure, and estimated that evolution occurred in these populations at rates “up to seven orders of magnitude greater than rates inferred from the paleontological record” (Resnick et al. 1997, p. 1934). Ashley et al. (2003) review evidence for rapid evolutionary changes in response to natural and anthropogenic agents in birds, fishes, mammals, lizards, and plants, with changes occurring in some cases within as little as a single year or generation.

In addition to its theoretical implications, the potential for rapid evolutionary change is critical to understanding how populations adapt to changing environments, for example in harvested or endangered populations where rapid changes in conditions can result from human management or lack thereof (Ashley et al 2003, Stockwell et al. 2003, Zimmer 2003). A change in extrinsic factors affecting mortality or reproductive success – such as a change in harvesting rate or juvenile survival – is necessarily a change in the forces of natural selection, and the response is likely to be modified by adaptation. Yet, based on the assumed separation of time scales (and despite evidence that commercial fishing has already led to significant evolutionary changes in harvested species), plans for species management rarely take into account the likelihood that ecological changes will evoke an evolutionary response (Stockwell et al. 2003, Ashley et al. 2003).

In this paper, we continue our studies of the interplay between ecological and evolutionary dynamics, focused on an experimental aquatic predator-prey system (Fussmann et al. 2000; Shertzer et al. 2002; Yoshida et al. 2003). Previous studies (summarized below) have shown that major properties of predator-prey oscillations in this system are determined by ongoing evolutionary dynamics in the prey population. Under other conditions, however, the predator and prey tend to apparently stable steady-state densities. These are the subject of the present paper. We study the previously developed model for our system under steady-state conditions, to determine how evolution shapes properties of the steady states. Specifically, we ask:

1. Under what conditions do we expect to find single versus multiple genotypes main-

tained by selection, and which ones?

2. To what extent does evolution affect the responses of the system to changes in external conditions such as resource availability and extrinsic sources of mortality?

The idea that evolution can affect ecological dynamics is certainly not new, indeed a substantial body of theory (reviewed by Abrams 2000) has developed over several decades to predict how the dynamics and stability of predator-prey interactions can be affected by trait evolution, and how selective harvesting can affect evolution in fish populations (Law and Grey 1989). However, key assumptions of the models have rarely been verified experimentally, and the practical difficulties of monitoring long-term changes in population abundances and trait distributions in order to test model predictions “has left a rather unfortunate gap between theory and experiment” (Abrams 2000, p. 98). “Although over 40 years of theory have addressed how evolutionary processes can affect the ecology of predator-prey interactions, few empirical data have addressed the same issue” (Johnson and Agrawal 2003). In the absence of an empirical foundation, there has been a proliferation of speculative models and a corresponding proliferation of alternative predictions: “Evolution can stabilize or destabilize interactions . . . When population cycles exist, adaptation may either increase or decrease the amplitude of those cycles” (Abrams 2000). In a general model of a 3-species (resource, consumer, predator) food chain, Abrams and Vos (in press) have shown that, as a result of adaptive changes in the consumer, an increase in consumer mortality rate could result in either an increase or a decrease in the resource, consumer (prey), and predator steady state values.

Our motivation for adding to this literature is to develop specific predictions for an experimentally tractable system, where model assumptions and predictions can be tested with quantitative rigor, allowing direct feedbacks between theory and experiment as in our previous studies with this system (Fussmann et al 2000, Shertzer et al. 2002, Yoshida et al. 2003). Experimental tests of theoretical predictions are strongest when predictions have been put on record *before* the experiments are done (Nelson G. Hairston, Sr., *personal communication*). We begin by describing the experimental system and model. We then analyze the model using approaches from evolutionary game theory – that is, under a given set of experimental conditions we seek to identify either single ESS prey genotypes (ESS=evolutionarily stable strategy) that cannot be invaded by any alternative genotype, or a non-invasible ESC of coexisting genotypes (ESC=evolutionarily stable combination). We then use the results of this analysis to predict how population response to changing conditions will be modified by adaptive changes in the prey.

The model can produce a wide range of dynamical behaviors depending on parameters. A

complete analysis of its behavior would be quite lengthy, but also not germane for empirical studies. We therefore consider a wide range of values for parameters that are under experimental control, but for parameters characterizing the organisms we restrict the analysis to values near those estimated to hold in our system. Note that experimental conditions leading to population cycles require a totally different analysis which will be the subject of a later paper.

1.1 Experimental system

The experimental system is a predator-prey microcosm with rotifers, *Brachionus calyciflorus*, and their algal prey, *Chlorella vulgaris*, cultured together in nitrogen-limited, continuous flow-through chemostat systems. *Brachionus* in the wild are facultatively sexual, but because sexually produced eggs wash out of the chemostat before offspring hatch, our rotifer cultures have evolved to be entirely parthenogenic (Fussmann *et al.* 2003). The algae also reproduce asexually (Pickett-Heaps 1975), so evolutionary change occurs as a result of changes in the relative frequency of different algal clones.

Two parameters of the system can be set experimentally: the concentration of limiting nutrient [nitrate] in the inflowing culture medium N_I , and the dilution rate δ , the fraction of chemostat medium that is replaced each day. A simple ordinary differential equation model given below is able to capture the experimentally observed qualitative behavior of the system: equilibria at low dilution rates, followed by cycling, followed by equilibria and then extinction (Fussmann *et al.* 2000) as the dilution rate is increased. However, the experimental system exhibited longer-period cycles and unique phase relations which did not match the short-period cycles and classic quarter-cycle predator-prey phase relations predicted by the model. Furthermore, the observed cycles showed extended periods where algal densities were high yet rotifer numbers remained low, followed by rapid growth in the rotifer populations while algal densities remained roughly unchanged.

A series of models were devised to explain these observations (Shertzer *et al.* 2002), each including some biologically plausible mechanism: rotifer self-limitation via reduced egg fitness when food is scarce; changes in algal nutrient composition as a function of nutrient availability; changes in algal physiology due to accumulation of toxins released by rotifers, and evolved prey defense against rotifer predation. Only the model including prey evolution was able to account well for the qualitative properties of the observed cycles. In that model, algae exposed to rotifer predation pressure evolved a “low palatability” phenotype at some cost to their competitive fitness. Subsequent experiments confirmed the existence of an evolutionary tradeoff between defense against predation and “fitness” (growth rate in absence

Table 1. Model Parameters

Parameter	Description	Value	Reference
N_I	Concentration of limiting nutrient in supplied medium	$80\mu \text{ mol N/l}$	Set
δ	Chemostat dilution rate	variable (d)	Set
V	Chemostat volume	$0.33l$	set
χ_c	Algal conversion efficiency	variable	fitted
χ_b	Rotifer conversion efficiency	variable	fitted
m	Rotifer mortality	$0.055/d$	F2000
λ	Rotifer senescence rate	$0.4/d$	F2000
K_c	Minimum algal half-saturation	$4.3 \mu \text{ mol N /l}$	F2000
K_b	Rotifer half-saturation	$0.835 \times 10^9 \text{ algal cells /l}$	
β_c	Maximum algal recruitment rate	$3.3/d$	TY
ω_c	N content in 10^9 algal cells	$20.0 \mu \text{ mol}$	F2000
ϵ_c	Algal assimilation efficiency	1	F2000
G	Rotifer maximum consumption rate	$5.0 \times 10^{-4} l/d$	TY
α_1	Shape parameter in algal tradeoff	variable, $\alpha_1 > 0$	fitted
α_2	Scale parameter in algal tradeoff	variable, $\alpha_2 > 0$	fitted

Set: Adjustable experimental parameter

F2000: Fussmann *et al.* 2000

TY: Yoshida *et al.*, in prep.

of rotifers): “grazed” algae grown under constant rotifer predation pressure were smaller, competitively inferior, and constituted inferior food (i.e., rotifers grew poorly when fed upon these cells) relative to “ungrazed” algae grown in rotifer-free environments (Yoshida *et al.*, submitted). Phenotypic differences between grazed and ungrazed algal lineages were heritable – persisting in subsequent generations grown under common conditions – demonstrating that the algal population evolved in response to grazing pressure. Experiments also verified the prediction that predator-prey cycles would exhibit very different qualitative properties (shorter period, and different phase relations) in the absence of prey evolution (Yoshida *et al.* 2003).

2 Description of the Model

The model is a system of ordinary differential equations describing the predator-prey and prey evolutionary dynamics in our microcosms. It is essentially the same as the model used by Yoshida *et al.* (2003), with minor simplifications for the sake of analytic tractability. The possibility for genetic variability and evolution in the algal prey population is modeled

by explicitly representing the algal population as a finite set of asexually reproducing clones. Each clone is characterized by its “food value” to the rotifers, denoted p (for “palatability”). Food value is defined by its effect on the rotifers: p can be thought of as the conditional probability that an algal cell is digested rather than ejected, once it has been ingested. The model thus consists of three equations for the limiting nutrient and rotifers, plus q equations for a suite of q algal clones. In the following equations, N is nitrogen (μ mol per liter), C_i represents concentration (per liter) of the i^{th} algal clone, where $i = 1, 2, \dots, q$; and R and B are *Brachionus*, fertile and total population counts in individuals per liter, respectively. Fecund rotifers senesce and stop breeding at a rate λ ; all rotifers are subject to fixed mortality m . The parameters χ_c, χ_b are conversions between consumption and recruitment rates (additional model parameters are defined in Table I).

$$\frac{dN}{dt} = \delta(N_I - N) - \sum_{i=1}^q F_{C,i}(N)C_i \quad (1)$$

$$\frac{dC_i}{dt} = \chi_c F_{C,i}(N)C_i - F_{b_i}(C_i)B - \delta C_i \quad (2)$$

$$\frac{dR}{dt} = \chi_b \sum_{i=1}^q F_{b_i}(C_i)R - (\delta + m + \lambda)R \quad (3)$$

$$\frac{dB}{dt} = \chi_b \sum_{i=1}^q F_{b_i}(C_i)R - (\delta + m)B \quad (4)$$

where

$$F_{c,i}(N) = \frac{\rho_c N}{K_c(p_i) + N} \quad (5)$$

and

$$F_{b_i}(C_i) = \frac{GC_i p_i}{K_b + \sum_{i=1}^q C_i p_i}. \quad (6)$$

are functional responses describing algal and rotifer consumption rates, respectively, and where $\rho_c = \frac{\omega_c \beta_c}{\epsilon_c}$.

Equation (6) is derived from the rotifer clearance rate \mathbf{G} (the volume of water per unit time that an individual filters to obtain food), which in this model is a function of algal food value:

$$\mathbf{G} = \frac{G}{K_b + \sum_{i=1}^q C_i p_i}.$$

That is, algae of lower value result in the rotifers increasing their clearance rate, exactly as if the density of food were lower. An alternate model in which rotifer clearance rate does not respond to food value was also considered, but could not fit the experimental data on

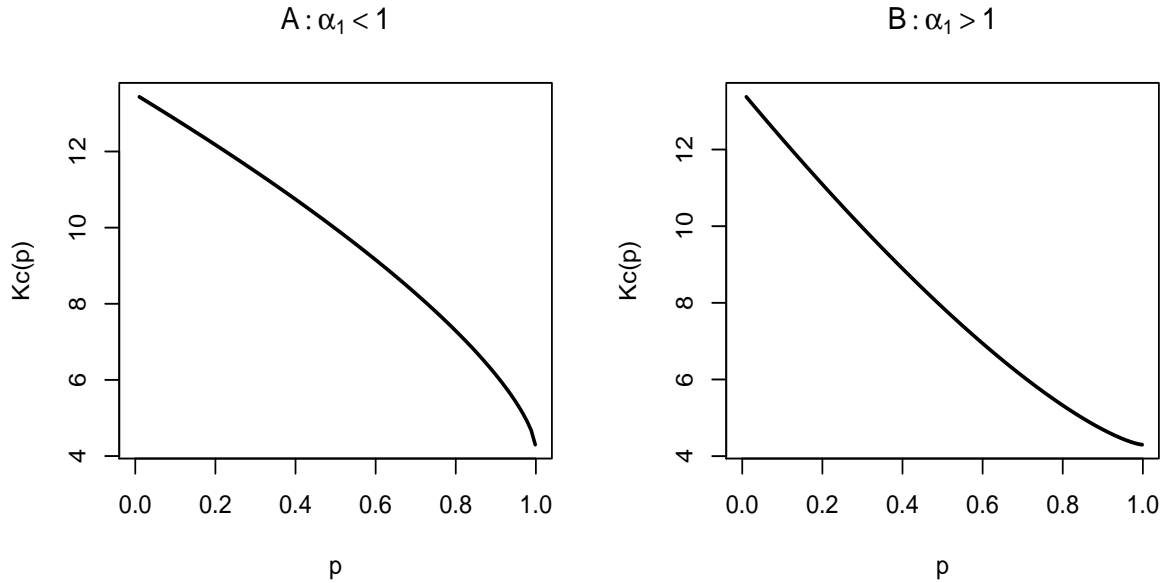


Figure 1: Plots of clonal food value, p versus half-saturation, $K_c(p)$ for shape parameter $\alpha_1 < 1$ (panel A) and $\alpha_1 > 1$ (panel B). When the tradeoff curve is concave *down* (left panel), it is more likely that surviving clones, either in equilibrium or in a cycling regime, represent two extremes in food value. When the curve is concave *up* (right panel), intermediate algal types can persist.

population cycles as well.

Each algal clone c_i is assigned a food value p_i between 1 (“good”) and 0 (“bad”), with lower p_i resulting in reduced risk of predation. A reduced food value comes, however, at the cost of reduced ability to compete for scarce nutrients. This relationship is specified by a tradeoff curve [Figure 1], modified from Yoshida *et al.* 2003. For simplicity, we use a two-parameter family to model how K_c varies between $p_i = 0$ and $p_i = 1$:

$$K_c(p_i) = K_c + \alpha_2(1 - p_i)^{\alpha_1}$$

where $K_c > 0$ is the minimum half-saturation value and $\alpha_1, \alpha_2 > 0$ are shape and cost parameters, respectively.

For most parameters we have fairly secure values based on direct experimental measurements (Table 1). For example, the parameters defining rotifer feeding rate were estimated by allowing known numbers of rotifers to graze on algae at known initial densities, with algal density measured again after a fixed amount of feeding time (T. Yoshida, *unpublished*). For some parameters, however, we only have indirect estimates obtained by fitting the model to population count data – these parameters are described as “fitted” in Table 1. Specifically, parameters were chosen to match as closely as possible the amplitude and period of

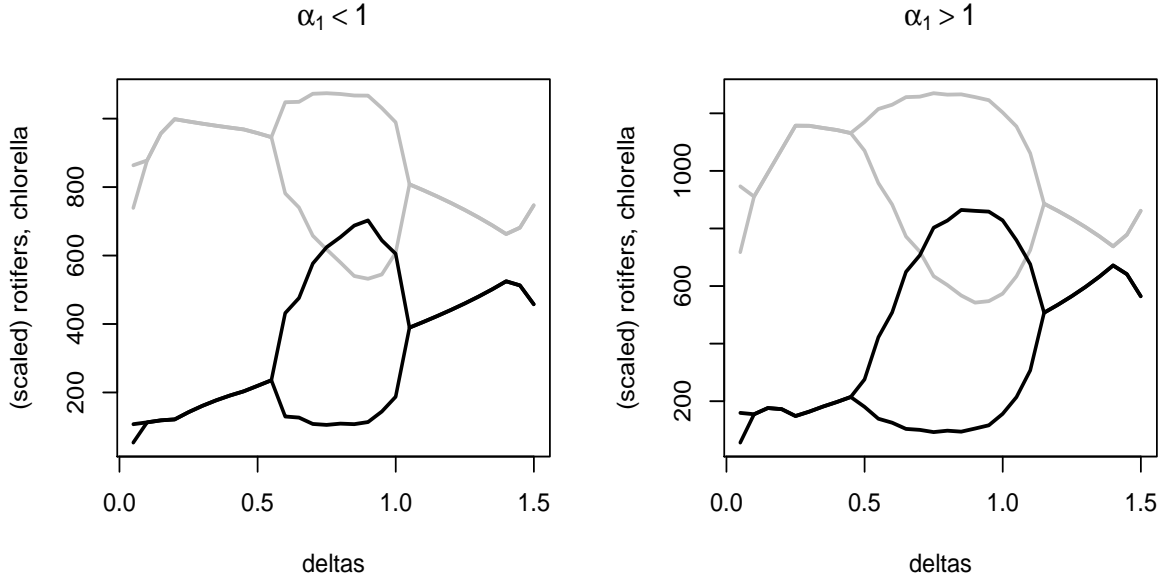


Figure 2: Numerical bifurcation diagrams for the clonal model. Population densities of algae (*Chlorella*) are shown in grey line; rotifers (*Brachionus*) in black line. Note the existence of equilibria at both low and high dilution rates. Predator-prey cycles occur at intermediate dilution rates. Parameter sets used in these calculations were obtained by simultaneous fitting of the clonal model [(1) – (6)] to amplitude, phase, and phase-lag observations from an intermediate dilution rate regime (i.e., $\delta = 0.69$), and a high dilution rate regime ($\delta = 0.96$) during which the system was cycling. Left panel, Phase diagram for tradeoff parameter $\alpha_1 < 1$: $\alpha_1 = 0.78$, $\alpha_2 = 9.4$, and $p_{min} = 0.10$. Right panel, Phase diagram for $\alpha_1 > 1$: $\alpha_1 = 1.35$, $\alpha_2 = 9.6$, and $p_{min} = 0.10$.

predator and prey cycles, and the phase lag between them, in experimental observations at two different dilution rates where the system exhibits cycles ($\delta = 0.69$ and $\delta = 0.96$), and to match the observed lack of cycles at low and high dilution rates. As is often the case, there is a range of parameter values more or less equally consistent with the data, and we explore how this parameter uncertainty affects our predictions. With the best-fitting parameter values, the model ((1)–(6)) produces a bifurcation diagram as a function of dilution rate, δ , which approximates the behavior our system exhibits in the laboratory (Fussmann et al. 2000, Yoshida *et al.* 2003, Supplementary material). “Low-flow” equilibria exist for dilution rates $\delta \approx 0.05 - 0.50$, followed by cycling at intermediate dilution rates, followed by “high flow” equilibria at $\delta \approx 1.0 - 1.5$ [Figure 2].

3 Analysis

3.1 Single-clone steady states

Assume now one dominant algal clone C with food value p . The model (1)–(4) then reduces to the following four equations, after substituting in the appropriate functional responses (5)–(6):

$$\begin{aligned}
 \frac{dN}{dt} &= \delta(N_I - N) - \frac{\rho_c NC}{K_c(p) + N} \\
 \frac{dC}{dt} &= \chi_c \frac{\rho_c NC}{K_c(p) + N} - \frac{GCpB}{(K_b + Cp)} - \delta C \\
 \frac{dR}{dt} &= \chi_b \frac{GCpR}{K_b + Cp} - (\delta + m + \lambda)R \\
 \frac{dB}{dt} &= \chi_b \frac{GCpR}{K_b + Cp} - (\delta + m)B.
 \end{aligned} \tag{7}$$

After some algebra, the steady state for (7) is found to be:

$$\begin{aligned}
 \bar{N} &= \frac{1}{2}[-\gamma + \sqrt{\gamma^2 + 4N_I K_c(p)}] \\
 \bar{C} &= \frac{K_b(\delta + m + \lambda)}{p(\chi_b G - (\delta + m + \lambda))} \\
 \bar{R} &= \frac{\delta \chi_b (\delta + m) [\chi_c (N_I - \bar{N}) - \bar{C}]}{(\delta + m + \lambda)^2} \\
 \bar{B} &= \frac{\delta \chi_b [\chi_c (N_I - \bar{N}) - \bar{C}]}{\delta + m + \lambda}
 \end{aligned} \tag{8}$$

where we define

$$\gamma = K_c(p) - N_I + \frac{\rho_c \bar{C}}{\delta}. \tag{9}$$

Note that these only hold for $\bar{B} > 0$. If p is too low or δ too high, the predators will be unable to persist, and the steady state nutrient and algal densities are

$$\begin{aligned}
 \bar{N} &= \frac{\delta K_c(p)}{(\chi_c \rho_c - \delta)} \\
 \bar{C} &= \chi_c (N_I - \bar{N})
 \end{aligned} \tag{10}$$

3.2 Conditions for ESS and ESC

We now ask under what conditions a particular clone C_r , with an associated food value p_r might be dominant and non-invasible. Following established usage, a clone C_r is said to

be an *Evolutionarily Stable Strategy* [ESS] if a population consisting of C_r , at steady state, cannot be invaded by a rare alternative clone C_i with food value p_i . The meaning of “rare” here is that the growth rate of a potential “invader” C_i is computed on the assumption that the population consists entirely of the “resident” type C_r . This quantity is now often called the *invasion exponent*, and is computed as follows:

$$\lambda(p_i|p_r) = \frac{1}{C_i} \frac{dC_i}{dt} = \frac{\chi_c \rho_c \bar{N}}{K_c(p_i) + \bar{N}} - \frac{G p_i \bar{B}}{(K_b + \bar{C}_r p_r)} - \delta \quad (11)$$

where \bar{N} , \bar{B} , \bar{C}_r are equilibrium conditions set by the resident. Note that $\lambda(p_i|p_i) \equiv 0$: pitted against itself, a clone neither increases nor decreases.

We can characterize ESSs by the first and second derivatives of the invasion exponent. To be an ESS, an interior trait value p^* (i.e., $p_{min} < p^* < p_{max}$) must satisfy both the first order condition, $\partial\lambda/\partial p_i = 0$ and second order condition, $\partial^2\lambda/\partial p_i^2 < 0$ at $p_i = p_r = p^*$. A trait value satisfying the first order condition will be called a *ESS candidate* (Ellner and Hairston 1994), because the first order condition is necessary but not sufficient. For the first order condition we have

$$\frac{\partial\lambda(p_i|p_r)}{\partial p_i} = \frac{\chi_c \rho_c \bar{N} \alpha_1 \alpha_2 (1 - p_i)^{(\alpha_1 - 1)}}{[K_c(p_i) + \bar{N}]^2} - \frac{G \bar{B}}{(K_b + \bar{C}_r p_r)}. \quad (12)$$

Setting $\bar{B}^* = \frac{G \bar{B}}{\chi_c \rho_c}$, we see that p^* is an ESS candidate if

$$\Omega_1(p^*) = \frac{\bar{N} \alpha_1 \alpha_2 (1 - p^*)^{(\alpha_1 - 1)}}{[K_c(p^*) + \bar{N}]^2} - \frac{\bar{B}^*}{(K_b + \bar{C}_r p^*)} = 0. \quad (13)$$

Taking the derivative of (12) with respect to the invader’s trait value, the second order condition is

$$\frac{\partial^2\lambda}{\partial p_i^2} = \xi_1 \{2\alpha_1 \alpha_2 (1 - p_i)^{\alpha_1} - (\alpha_1 - 1)[\bar{N} + K_c(p_i)]\}, \quad (14)$$

where

$$\xi_1 = \frac{\chi_c \rho_c \bar{N} \alpha_1 \alpha_2 (1 - p_i)^{(\alpha_1 - 2)}}{[K_c(p_i) + \bar{N}]^3} > 0$$

provided $0 \leq p_i < 1$. Thus, to be an ESS, an interior candidate p^* must also satisfy

$$g(p^*) = 2\alpha_1 \alpha_2 (1 - p^*)^{\alpha_1} - (\alpha_1 - 1)[\bar{N} + K_c(p^*)] < 0. \quad (15)$$

Where no single ESS exists – in particular when a candidate fails to satisfy the second order condition – it is often possible to identify a non-invasible ESC (Evolutionarily Stable Combination) of coexisting genotypes. An ESC κ of coexisting genotypes is characterized by the invasion exponent for an introduced rare type p_i ,

$$\lambda(p_i|\kappa) = \frac{1}{C_i} \frac{dC_i}{dt} = \frac{\chi_c \rho_c \bar{N}}{K_c(p_i) + \bar{N}} - \frac{G p_i \bar{B}}{(K_b + \bar{C}_\kappa)} - \delta \quad (16)$$

Table 2. Predicted evolutionary outcome as a function of the invasion exponents when $\alpha_1 < 1$.

	$\lambda(p_{max} p_{min}) > 0$	$\lambda(p_{max} p_{min}) < 0$
$\lambda(p_{min} p_{max}) > 0$	ESC $\kappa = \{p_{min}, p_{max}\}$	p_{min} is ESS
$\lambda(p_{min} p_{max}) < 0$	p_{max} is ESS	Both are (local) ESS

where \bar{N} , \bar{B} , are the steady state nutrient and rotifer densities set by κ and \bar{C}_κ is the “effective” algal density at the ESC steady state,

$$\bar{C}_\kappa = \sum_{j \in \kappa} p_j \bar{C}_j \quad (17)$$

If $\lambda(p_i|\kappa) < 0$ for all $p_i \notin \kappa$ then κ is an ESC. A more refined local classification of evolutionary stability is possible, also based on derivatives of the invasion exponent (Figure 1 of Levin and Muller-Landau (2000) summarizes the various stability concepts and their relationships), but the ESS and ESC concepts are sufficient for studying our model.

3.3 Shape parameter $\alpha_1 < 1$

We observe from (14) that

$$\frac{\partial^2 \lambda}{\partial p_i^2} > 0 \text{ when } \alpha_1 < 1. \quad (18)$$

Therefore no *interior* trait p (i.e., $p_{min} < p < p_{max}$) can be an ESS if $\alpha_1 < 1$. In addition there cannot be an ESC that includes any interior types (see the Appendix), so any ESC must consist of the extreme types $\{p_{min}, p_{max}\}$. The evolutionary outcome can therefore be determined from the two invasion exponents $\lambda(p_{min}|p_{max})$ and $\lambda(p_{max}|p_{min})$ [Table 2].

Recall that food value p is scaled so that $p_{max} \equiv 1$, representing the undefended clone that is favored when predators are absent. However, the evolutionary outcome may depend on the value of p_{min} , the food value corresponding to the highest possible level of defense. We consider below a wide range of possible values for p_{min} , i.e. we regard it as being under experimental control rather than a fixed property of the organism. Although the latter is literally true, p_{min} can be increased temporarily by using a restricted set of founding genotypes as in Yoshida et al. (2003).

Figure 3 shows plots of the invasion exponents $\lambda(p_{max}|p)$ and $\lambda(p|p_{max})$ (panels A and B), and the predicted outcome according to the criteria in Table 2 (panels C and D). In the low-flow regime (panel A), when p is near 0 both $\lambda(p_{max}|p)$ and $\lambda(p|p_{max})$ are positive. Thus, when p_{min} is in the range of p values where these inequalities hold, we predict an ESC. As p increases, $\lambda(p|p_{max})$ remains positive (dashed line) but $\lambda(p_{max}|p)$ becomes negative (solid line). For p_{min} in this range of p values, we therefore have $\lambda(p_{min}|p_{max}) > 0$ and

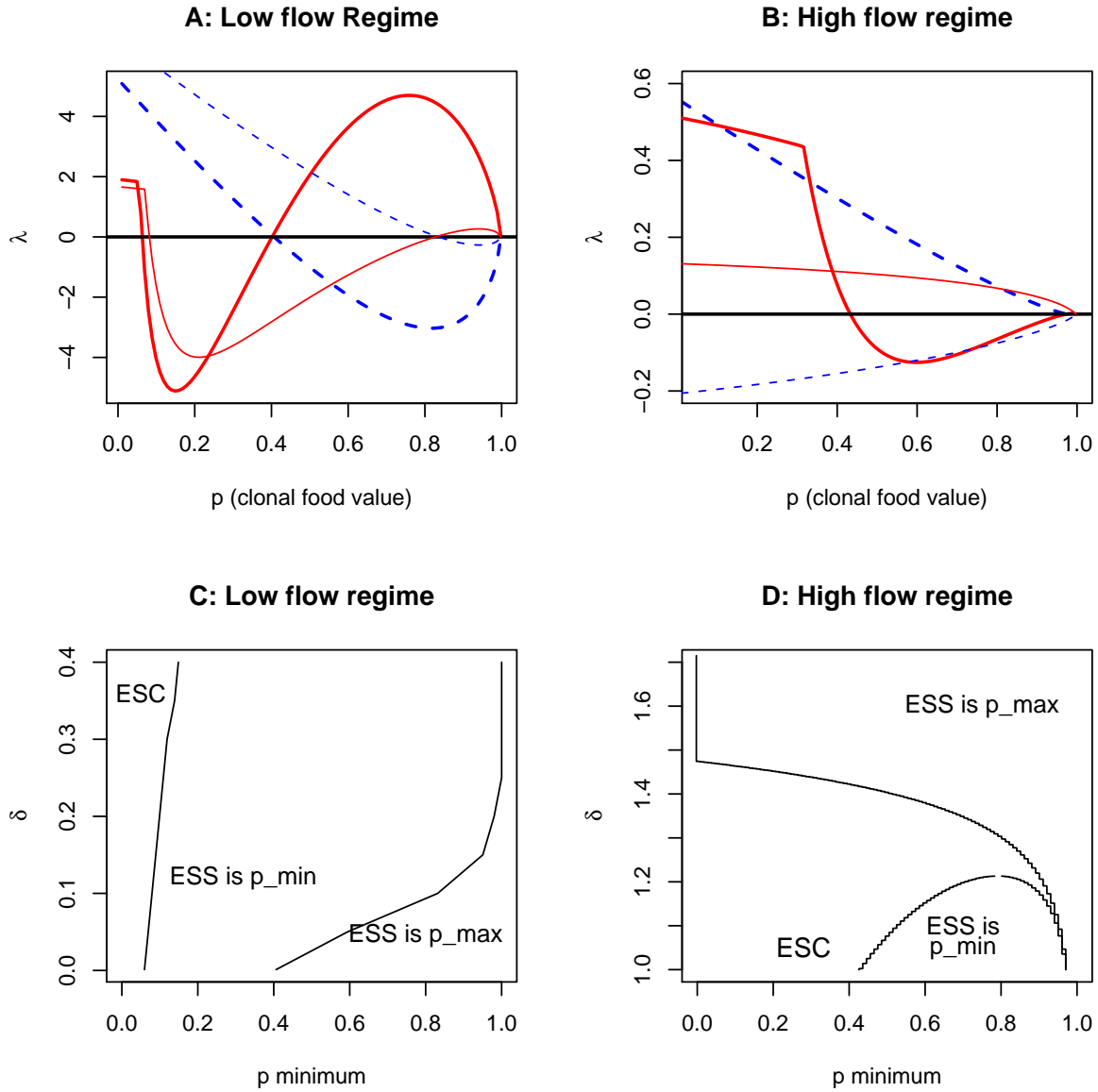


Figure 3: Invasion exponents and evolutionary steady states when $\alpha_1 < 1$. (A) Plots of the invasion exponents $\lambda(p_{max}|p)$ (solid line) and $\lambda(p|p_{max})$ (dashed line) as a function of p for low flow rates, $\delta = 0.001$ (bold) and $\delta = 0.15$ (thin). (B) As in panel (A) for high values of δ , $\delta = 1.0$ (bold) and $\delta = 1.7$ (thin). Panels (C) and (D) show the predicted evolutionary steady states that result from the plots in (A) and (B) using the criteria in Table 2, as a function of δ and p_{min} . The “corner” in the plot of $\lambda(p_{max}|p)$ occurs at the minimum food value p that allows persistence of the predators. Above this critical value, $\lambda(p_{max}|p)$ is calculated for a system steady state including N , C , and B ; below this critical value only N and C are present in the system at steady state.

$\lambda(p_{max}|p_{min}) < 0$, and the ESS is the minimum existing p (that is, the most defended clone). As p increases further the two exponents reverse in sign, so if p_{min} lies to the right of this change-point p_{max} is an ESS.

The high flow regime is shown in Figure 3 B. For p very near 1 the situation is the same as at low flow: $\lambda(p_{max}|p) > 0$ and $\lambda(p|p_{max}) < 0$, and we again have p_{max} as the ESS. As p decreases $\lambda(p_{max}|p)$ remains positive for dilution rates at the high end of the high flow regime, but becomes immediately negative as p decreases from p near 1 at the low end of the regime, i.e., for $\delta \doteq 1$. $\lambda(p|p_{max})$ may either remain negative or become positive, depending on the value of δ . When a sign-change occurs, $\lambda(p|p_{max})$ is positive and $\lambda(p_{max}|p)$ negative, and we have p_{min} as an ESS, or both exponents are positive so the predicted outcome is an ESC: a combination of the two extreme types. The location of the sign-change decreases with increasing δ , and eventually vanishes.

The plots shown in Figure 3 are specific to our parameter set, but we show in the Appendix that the relevant qualitative properties of these curves are robust to substantial variation in parameter values.

3.4 Shape parameter $\alpha_1 > 1$: analysis

The situation is more complicated if $\alpha_1 > 1$, because an internal ESS is then possible. We therefore need to analyze (in this Subsection) properties of the first and second order conditions for a local ESS. The implications for evolutionary steady states when $\alpha_1 > 1$ are presented in the next Subsection.

3.4.1 First order conditions

We return to the first order expression, $\Omega_1(p)$ (13), and search for ESS candidate types by exploring where (13) holds as a function both of clonal food value p^* and dilution rate δ , given $0 \leq p^* < 1$ and $\alpha_1 > 1$. Example calculations of $\Omega_1(p)$ as a function of trait value p , dilution rate δ , and rotifer conversion efficiency χ_b are shown in Figure 4. Each zero point in a curve corresponds to a ESS candidate associated with a given dilution rate, δ .

For very low dilution rates, $\Omega_1(p)$ converges to a limiting form shown in bold (Figure 4 A,C; bold line), for which, in this case, there are three ESS candidates. Depending on the value of the cost parameter, α_2 , the limiting form may either remain below the zero axis (low α_2 values, one ESS candidate), or loop above it (high α_2 values, three candidates) as in Figure 4 A. As dilution rate increases, the curve dips entirely below the p -axis (Figure 4 A,C; thin

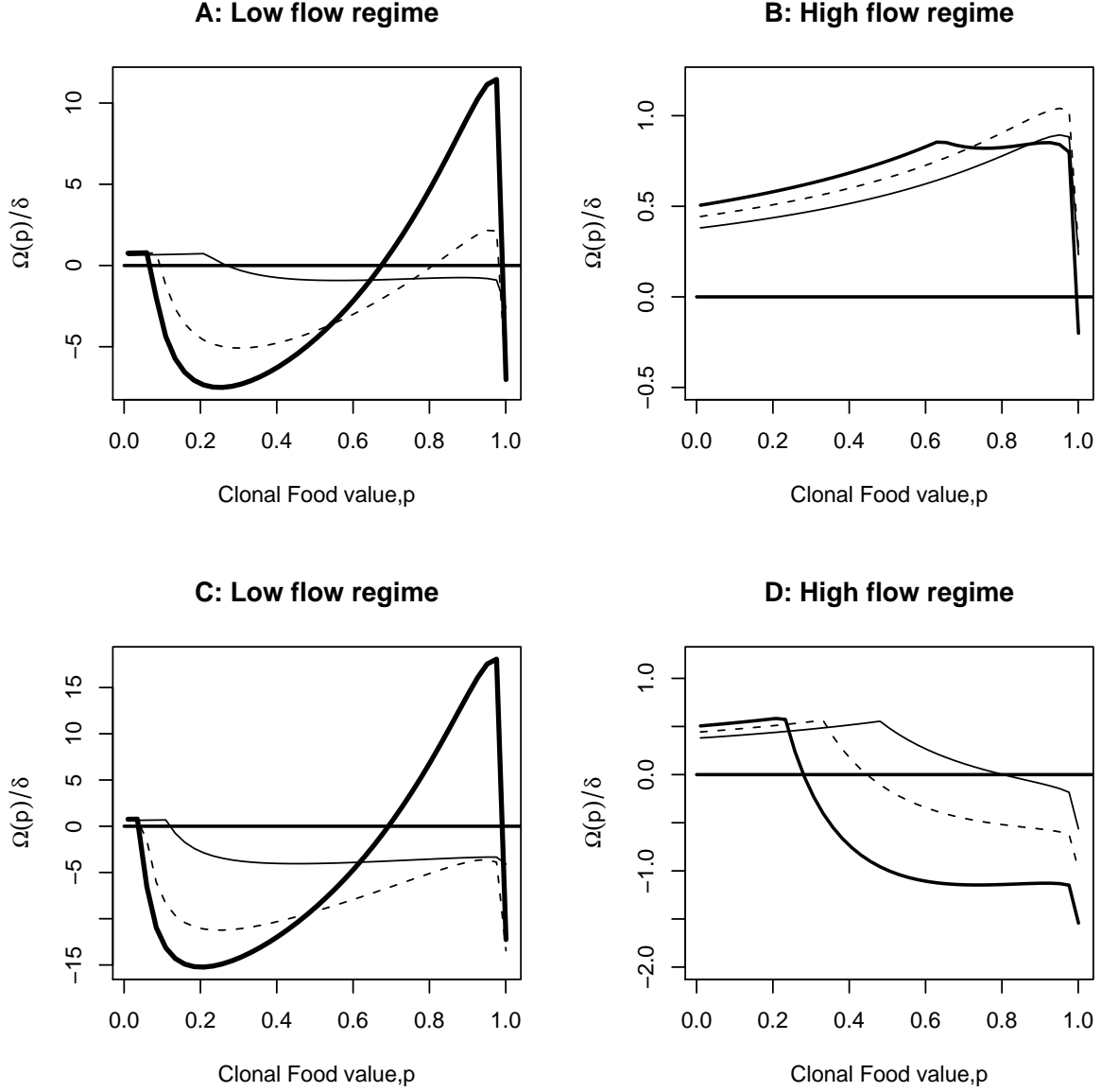


Figure 4: First order conditions (13) for the system when $\alpha_1 > 1$ (note that cost parameter $\alpha_2 = 9.8$ can be classified as “high” in value, so conditions for limiting dilution rate $\delta \rightarrow 0$ loop above the zero line). A, $\Omega_1(p)$ (13), scaled by dilution rate, δ is shown for the low dilution regime ($\delta = 0.1 - 0.5$) and conversion efficiency $\chi_b = 4000$ (thin line). The limiting form for $\delta \rightarrow 0$ is shown in bold line; representative curves for $\delta = 0.1$ and $\delta = 0.5$ are shown in thin dashed and solid line, respectively. B, $\Omega_1(p)$ for high dilution rates $\delta = 1.0 - 1.5$, $\chi_b = 4000$; curve for $\delta = 1.0$ is shown in bold; representative curves for $\delta = 1.25$ and $\delta = 1.5$ are shown in thin dashed and solid line, respectively. C, As in panel A for $\delta = 0.1 - 0.5$, $\chi_b = 6000$. Again, the limiting form for $\delta \rightarrow 0$ is shown in bold. D, As in panel B for $\delta = 1.0 - 1.5$ and $\chi_b = 6000$. Plots for $\delta = 1.0$ shown in bold. Note that in the high dilution rate regime, the ESS candidate values move from left to right as dilution rate increases.

dashed and solid line), and the two higher- p candidates move together, eventually colliding and vanishing. The trait value(s) of ESS candidates are little affected by variations in rotifer conversion efficiency χ_b in the low dilution regime (Figure 4 A,C). Note that both δ and χ_b enter the first order condition, $\Omega_1(p)$, through the steady state values \bar{N} , \bar{B} , and \bar{C}^* (8).

In the high dilution rate regime, there is a single ESS candidate which increases in p -value as dilution rate increases (Figure 4 B,D). Lower estimates of rotifer conversion efficiency result in higher p -value ESS candidates. For example, at $\chi_b = 4000$, an ESS candidate exists at $p \approx 1$ for $\delta = 1.0$ (Figure 4 B, heavy line). However, at $\chi_b = 6000$, the candidate for the dilution rate $\delta = 1.0$ sits at $p \approx 0.3$ (Figure 4 D, heavy line). Higher conversion efficiencies result in greater numbers of rotifers, increased selection for defense, and thus a lower p -value ESS candidate.

Most noticeably at higher dilution rates, varying α_1 also affects the position of the ESS candidate. If α_1 is increased from some initial value $\alpha_1 > 1$, candidate p values shift to the left. This is sensible when one considers the effect of an increase or decrease in α_1 on the trade-off curve. Increasing α_1 makes the curve more deeply concave upwards, while decreasing α_1 flattens it. As the curve becomes more deeply concave upwards, one might expect surviving clones to migrate in p -value towards the middle of the curve, and as it flattens, to move to the extremes – thus, for high p -values, to shift towards the high- p endpoint.

3.4.2 *Second order conditions*

Second order conditions (15) are strongly affected by variation in several parameters, most notably shape parameter α_1 , rotifer conversion efficiency χ_b , and dilution rate δ . In the Appendix we demonstrate that g is a decreasing function of both α_1 and χ_b ; a decreasing function of δ in the low dilution range, but an increasing function of δ in the high dilution range. Consequently, increases in either α_1 or χ_b shift the second order curve to the left (at a given dilution rate, δ), so that lower p value candidates satisfy the second order condition. Conversely, decreasing either α_1 or χ_b will shift the curve to the right, so that only high p value candidates, can satisfy the second order condition.

The behavior of g with increasing δ implies that ESS candidates must shift to the right as a function of δ in order to satisfy the second order condition (15). All else being held constant, for $\alpha_1 > 1$, only relatively high- p , high- δ candidates thus satisfy both the first order (13) and second order conditions. An internal ESS may exist at high δ equilibria, depending on conversion efficiency χ_b , but not at low δ equilibria.

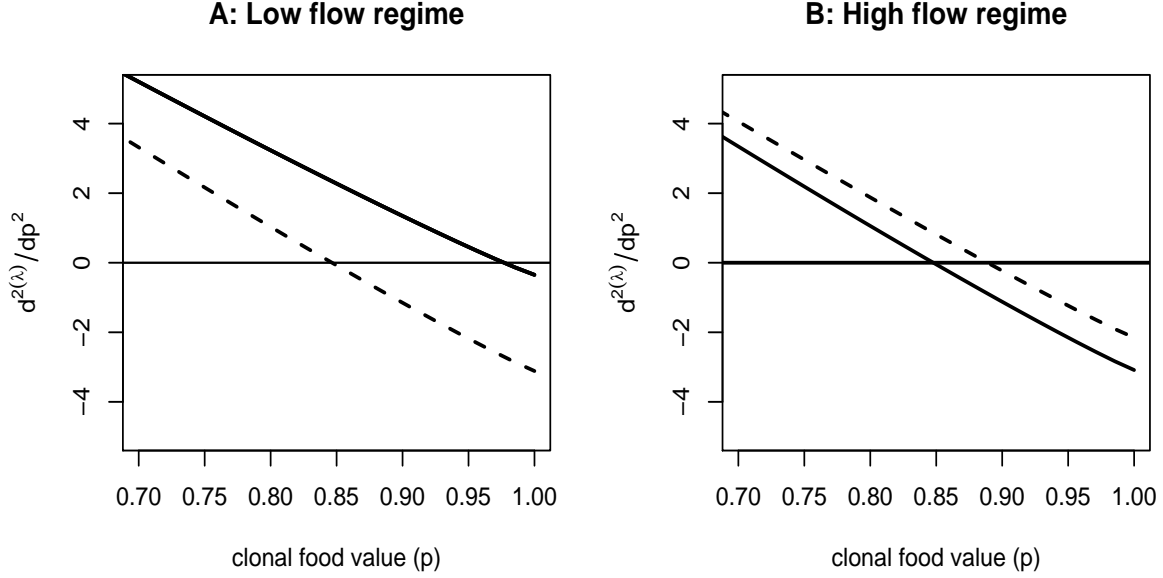


Figure 5: Second order conditions (15) for the system when $\alpha_1 > 1$. Curves represent second order conditions as a function of p^* for equilibrium dilution rates $\delta = (0.1 - 0.5; 1.0 - 1.5)$. A: second order conditions for low dilution rate regime $\delta = 0.1 - 0.5$. Dashed lines show curves for $\delta = 0.1, 0.5$. Heavy bold line shows the limiting form (15) assumes at very low δ (i.e., $\delta < O(10^{-3})$). B: second order conditions for the high dilution rate regime $\delta = 1.0 - 1.5$. In bold line is shown the curve for $\delta = 1.0$; dashed line shows curve for $\delta = 1.5$

Plotting (15) as a function of p and δ , we see that low- δ , low- p candidates invariably fail the second order condition, because $g(p^*)$ remains positive for these candidates (Figure 5). For very low (limiting) δ , there may be high- p candidates which satisfy the second order condition; cf. Figure 4, panels A, C, bold line. The presence or absence of these candidates depends primarily on cost parameter α_2 , as discussed in the next section. However, as δ increases, the ESS candidate shifts to higher p -values, and for these values of p^* , $g(p^*)$ becomes negative. Thus while an internal ESS may exist at high dilution equilibria, there is no internal ESS at low dilution rates: a low dilution rate ESS, if it exists, must be an endpoint value.

3.5 Shape parameter $\alpha_1 > 1$: Results

We now use the results above to identify the form of the evolutionary steady states for $\alpha_1 > 1$. Figure (6) summarizes the results. Panels A through D show first and second order conditions for this system together on one plot: solid lines indicate ESS candidates, which we'll call p^* , and the dashed line is a plot of the second order condition $g(p^*)$ (15). To the left of the dashed line, ESS candidates fail the second order condition; to the right of this

line, candidates satisfy this condition. Note that first order conditions for the parameters in 6 A, B are found in 4 C, D.

For a low flow regime with high cost parameter value α_2 and for p small, there are ESS candidates, p^* (solid line, panel A), but they fail the second order condition. Then, for $p_{min} < p^*$, there is thus an ESC of the two extreme types in proportions such that the ESC has an average p value approximating the ESS candidate value, p^* . For $p_{min} > p^*$, the first order condition becomes negative and all clones are invisable by p_{min} , which forms an endpoint ESS. For the high cost-value ($\alpha_2 \doteq 10$) example shown in panel A, there is an additional set of high p ESS candidates at very low dilution rate. However, simulations indicate that these candidates form only a very local ESS and may be invaded by lower p clones. Note that if the cost parameter is lower (e.g., $\alpha_2 = 4$, panel C), these high p , low δ ESS candidates do not occur, and only the ESC and low- p endpoint ESS are observed.

In the high-flow regime, ESS candidates p^* generally increase in p -value with increasing dilution rate (panels B and D, solid line). For this parameter set, however, all ESS candidates for $\delta < 1.35$ fail the second order condition. Thus, for $p_{min} < p^*$, there is again an ESC of p_{min} and p_{max} , in proportions such that the average p value approximates the candidate value p^* (panel B). For $p_{min} > p^*$, the first order condition becomes negative, so higher p clones are invisable by $p_{min} > p^*$, and p_{min} is again an endpoint ESS. However, where ESS candidates do not fail the second order condition, in this case for $\delta > 1.35$, an internal ESS exists (above dotted line, panel B). Recall that as α_1 is increased, we have shown that the second order curve $g(p^*)$ shifts to the left. In this example this causes the intersection between the first and second order curves (dotted line, panel D), to occur at lower and lower dilution rates. Thus more and more of the high dilution rate regime has an internal ESS.

Recalling that shape parameter α_1 and assimilation efficiency χ_b affect first and second order conditions at high dilution rates, we turn to a second example (panels C,D). Here both α_1 and χ_b have been increased. Increasing α_1 shifts ESS candidate values to the left, as does increasing χ_b . However, this example also features a lower cost parameter ($\alpha_2 \sim 4$), which *steepens* the first order line such that all ESS candidate types fail the second order condition for these parameters. Thus as above, for $p_{min} < p^*$, there is an ESC centered about the ESS candidate value, and for $p_{min} > p^*$, p_{min} forms an endpoint ESS. Since ESS candidates fail the second order condition for all dilution rates, an internal ESS never exists. The results are otherwise the same as in panel B.

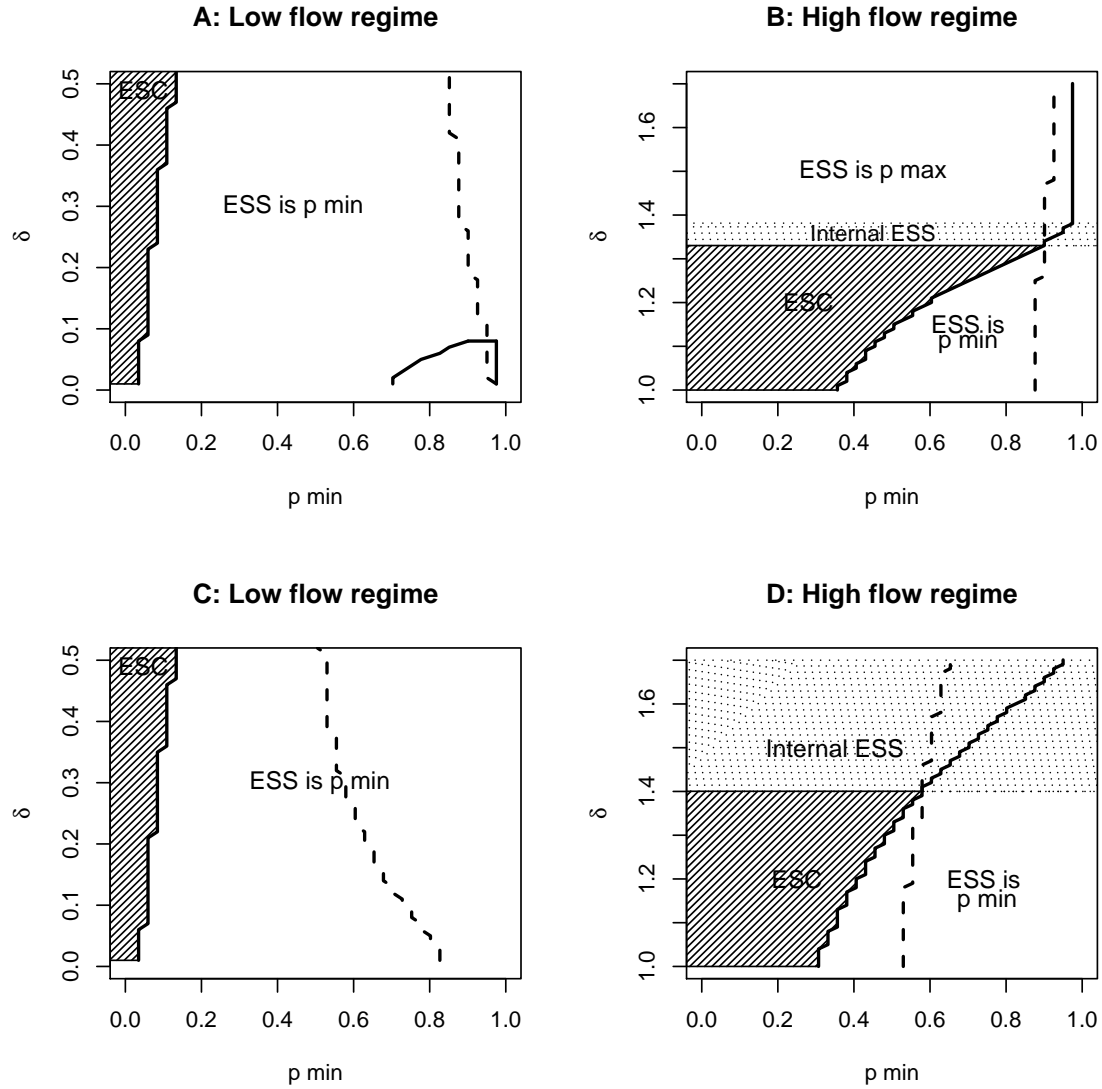


Figure 6: Evolutionary steady states when $\alpha_1 > 1$. ESS candidates are shown in solid line; to the *right* of the dashed line the second order condition $\frac{\partial^2 \lambda}{\partial p_i^2} < 0$ is satisfied, so a candidate is an ESS if it lies to the right of the dashed line. If p_{min} lies to the left of the ESS candidate line, the evolutionarily stable state is either an ESS (if the candidate satisfies the second order condition) or an ESC (if the candidate does not satisfy this condition). Parameters for system shown in panels A-B: $\alpha_1 = 1.08$, $\alpha_2 = 9.8$, $\chi_b = 5420$; panels C-D: $\alpha_1 = 1.19$, $\alpha_2 = 3.9$, $\chi_b = 6055$.

4 Simulations

Since results from the type of ESS analysis we have just completed may only hold locally, we tested our analytical conclusions by performing simulations of the system (1)-(6). The simulations were written in the **R** language (version 1.7) and run on a Windows 2000 platform, using the **odesolve** package. Tests were performed for a representative sample of parameter sets with $\alpha_1 < 1$ and $\alpha_1 > 1$ and in a range of dilution rates, as follows.

First, summary diagrams, such as those shown in Figure 3 C,D (for $\alpha_1 < 1$) and Figure 6 A-D (for $\alpha_1 > 1$), were created to show the predicted evolutionary equilibria for each parameter set. Then, each diagram was “gridded” coarsely in (p_{min}, δ) and simulations of the system in equations (1)-(6) were run to verify the analysis at each grid point. Some additional “spot-check” simulations were used to look more closely at predicted transition points, e.g. from ESC to ESS. In each case, the system included an initial set of 40 clones, distributed evenly in p value along the tradeoff curve determined by the parameter set in question. After running a given simulation, we examined time-series trajectories for C , total *Chlorella* cell counts; average palatability p ; normalized clonal frequency c_i as a function of time; and mean clonal frequency as a function of p . Each run verified that (1) the system was in equilibrium (p_{min} is a bifurcation parameter, thus equilibrium must be repeatedly confirmed as p_{min} varies); and (2) the clone or clones identified by analysis were indeed dominant. In only one case, noted above, did we find that an ESS identified by our analysis was only local in nature, and thus invisable by clones of much lower p value.

5 Evolution and response to changing conditions

We can now return to the question posed in the Introduction: how important is an understanding of evolutionary dynamics for making quantitative predictions of how the system will respond to “management” (an externally imposed alteration in conditions)? If, as the preceding analysis and examples suggest, a change in conditions results in a change in community composition, then predictions of how such a community might respond to management must not omit the effects of evolution.

Figure 7 shows predicted responses of the system with and without evolution to changes in the dilution rate, which affects both nutrient supply and mortality rates. In panels A,B we assume $\alpha_1 < 1$, and evolutionary dynamics are as summarized in Figure 3 C. In both panels, the dashed line shows the effects on *Chlorella* density assuming the system responds to external change by evolving, while solid line shows the predicted response if effects of

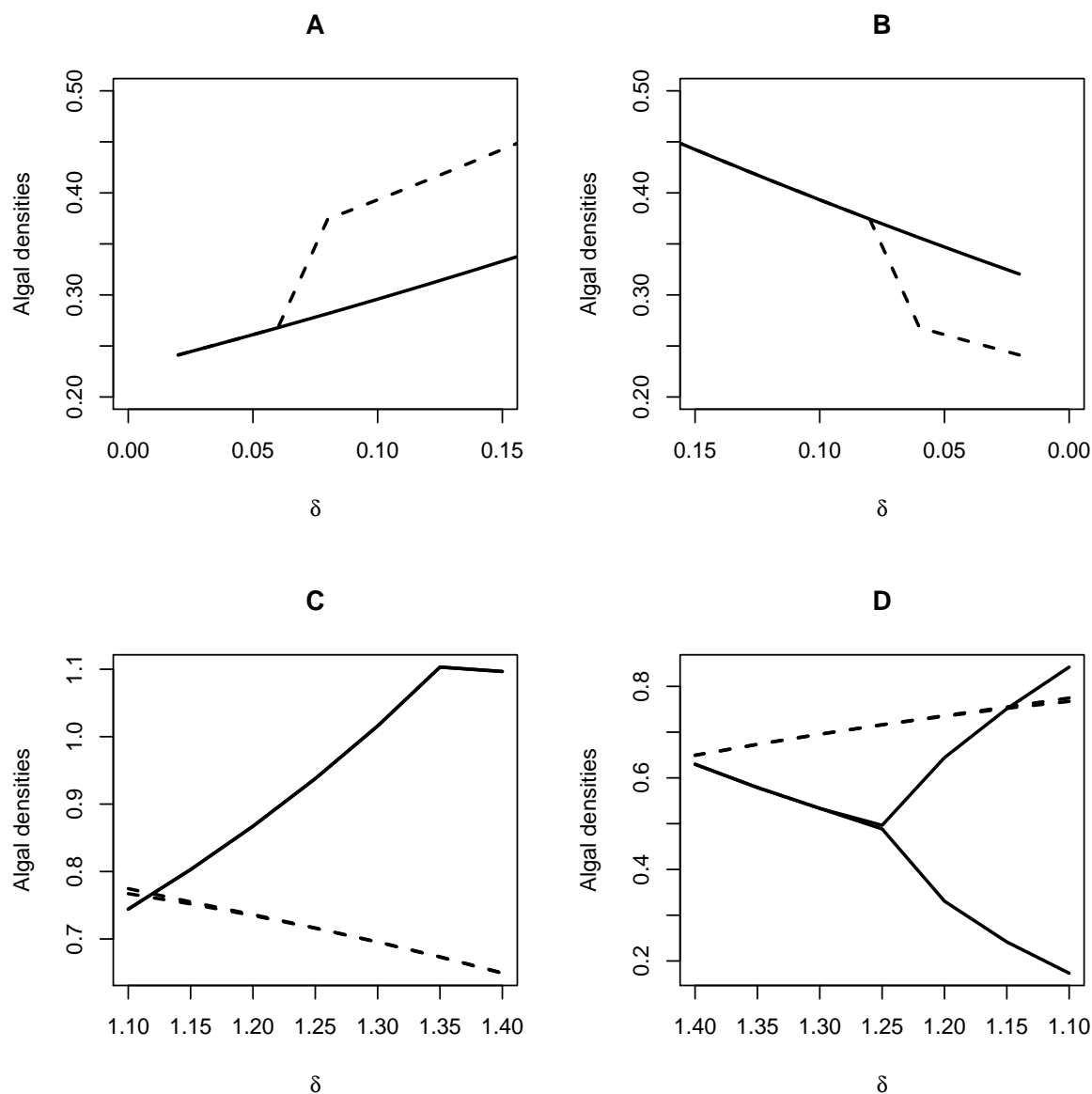


Figure 7: Effects of change in dilution rate on steady-state algal density in an evolutionarily dynamic system versus a static (non-evolving) system, for $\alpha_1 < 1$ (panels A, B) and $\alpha_1 > 1$ (panels C, D). Panels A, B: $p_{min} = 0.75$; solid line shows static response, and dashed line shows dynamic response. Parameters and evolutionary dynamics are as in Figure 3 C. A, Initial dilution rate $\delta = 0.02$, increased to $\delta = 0.15$. B, Initial dilution rate $\delta = 0.15$, decreased to $\delta = 0.02$. Panels C, D: parameters and evolutionary dynamics are as in Figure 6 D. The dynamic system (dashed line) includes 40 clones; the static system (solid line) is a single-clone whose parameters reflect the aggregate properties of the ESC. C, Initial dilution rate $\delta = 1.1$, increased to $\delta = 1.4$. D, Initial dilution rate $\delta = 1.4$, decreased to $\delta = 1.1$.

evolution are ignored. In panel A we set $p_{min} = 0.75$, then slowly increase the dilution rate from $\delta = 0.02$ to $\delta = 0.15$, thus crossing from “ESS is p_{max} ” to “ESS is p_{min} ” on Figure 3 C. Both systems respond identically initially, but at the “transition” dilution rate ($\delta \doteq 0.8$ for this choice of parameters), population densities in the evolutionarily dynamic treatment suddenly increase to a higher steady-state (dashed line), while those in the static treatment follow the original (solid line) steady-state. In both systems the initial dominant was p_{max} , but only the evolutionarily dynamic system shifted to the more competitively fit dominant type, p_{min} .

In panel B we run the converse experiment: we set $p_{min} = 0.75$, but start at dilution rate $\delta = 0.15$. We then decrease the dilution rate slowly back down to $\delta = 0.02$, thus passing back from “ESS is p_{min} ” (Figure 3 C) to “ESS is p_{max} ”. Both systems begin with p_{min} as dominant and their response is identical, but as dilution rate passes through the transition at $\delta \doteq 0.08$, the evolutionarily dynamic system switches to p_{max} as dominant, resulting in lower algal densities (dashed line). The evolutionarily static system continues to be dominated by p_{min} (solid line). So up to a point, the system’s response to changing conditions can be predicted without regard to the underlying evolutionary dynamics, but then a rapid evolutionary response to a small change in conditions causes a discontinuous response that would not be predicted when evolutionary dynamics are ignored.

With $\alpha_1 > 1$ (Figure 7C,D) there is an immediate divergence between the actual system response, and predictions that ignore the effect of evolution. Again, in both panels, the solid line shows the response of an evolutionarily static system, and in dashed line is the response of the evolutionarily dynamic, multiple clone system. In panel C we choose an initial dilution rate of $\delta = 1.10$, and slowly increase the dilution rate to $\delta = 1.4$. At the initial dilution rate, the multiple clone system has an ESC comprised of the extremes, p_{min} and p_{max} , in proportions such that their average p value approximates the ESS candidate at that dilution rate. Algal densities (dashed line) slowly fall as dilution rate increases, due to an increase in average p value of the ESC with increasing dilution rate (higher δ reduces the rotifer density, and thus reduces the selection for unpalatability). The evolutionarily static system has a single clone, whose parameters reflect the aggregate properties of the ESC (for example, its value of K_c was set to the nutrient concentration at which the total uptake rate of the ESC clone mix reached half its maximum value). Here, higher dilution does not evoke the evolutionary response of increased palatability in the prey, so rotifers begin to drop out of the system almost immediately, with a consequent steady increase in algal densities (solid line). By $\delta = 1.35$, the rotifers are extinct, and algal densities stabilize.

We then run our imaginary experiment the other way (Figure 7 D), selecting an initial dilution rate of $\delta = 1.4$, and slowly decreasing the dilution rate back down to $\delta = 1.1$.

The dynamic system responds to a decrease in dilution rate with a slow increase in algal densities: this is because the average palatability of clones comprising the ESC is decreasing with δ , with the expected effect on rotifer abundances. The static system (a single clone mimicking the aggregate properties of the ESC at $\delta = 1.4$) maintains constant palatability as conditions change, and again its response is very different from the outcome when evolution occurs (note that the system begins to cycle as we pass back through a bifurcation point at $\delta \doteq 1.25$).

We now propose a set of experimental checks for our analysis that are robust to parameter uncertainties, and in particular to the shape of the tradeoff curve. A general prediction for any plausible parameter values is that the evolutionary steady-state at very high dilution rates is a single clone (either p_{max} or an ESS near p_{max}), which is replaced by an ESC as the dilution rate decreases. As dilution rate decreases further, a Hopf bifurcation occurs and the attractor is then a limit cycle. The nature of the cycles (their period and the phase lag between predator and prey) depends on which prey clones are present (Yoshida et al. 2003).

We therefore predict that if the dilution rate is quickly dropped into the limit-cycle regime, the nature of the cycles will (at least initially) depend on the prior dilution rate and evolutionary steady state. Figure ?? shows this scenario for both $\alpha_1 < 1$ (panels A, B) and $\alpha_1 > 1$ (panels C, D). In panel A ($\alpha_1 < 1$), we start with an initial dilution rate of $\delta = 1.15$. The predicted outcome is an ESC of the extreme types, p_{min} and p_{max} (Figure ?? D). After equilibrium is established, we abruptly step down the dilution rate to $\delta = 0.70$. Given the presence of two very different clones, we predict longer cycles with algal and rotifer peaks exactly out of phase (Yoshida et al. 2003). In panel B we start with dilution rate $\delta = 1.65$, at which we expect an ESS of p_{max} (Figure ?? D). When the dilution rate is stepped down to $\delta = 0.70$, short cycles with classical predator-prey phase relations result, as one would expect from a single-clone system (Yoshida et al. 2003). Panels C and D show a corresponding step-down experiment for $\alpha_1 > 1$. In both cases, the nature of the cycles that occur immediately after the step-down reveals the genetic diversity that was present before the step-down, and thus lets us test our predictions about the “hidden” prey diversity at steady-state. Note, however, that prey evolution continues to occur after the step-down (panel D), so only the transient behavior after the step-down is revealing of prior evolutionary history.

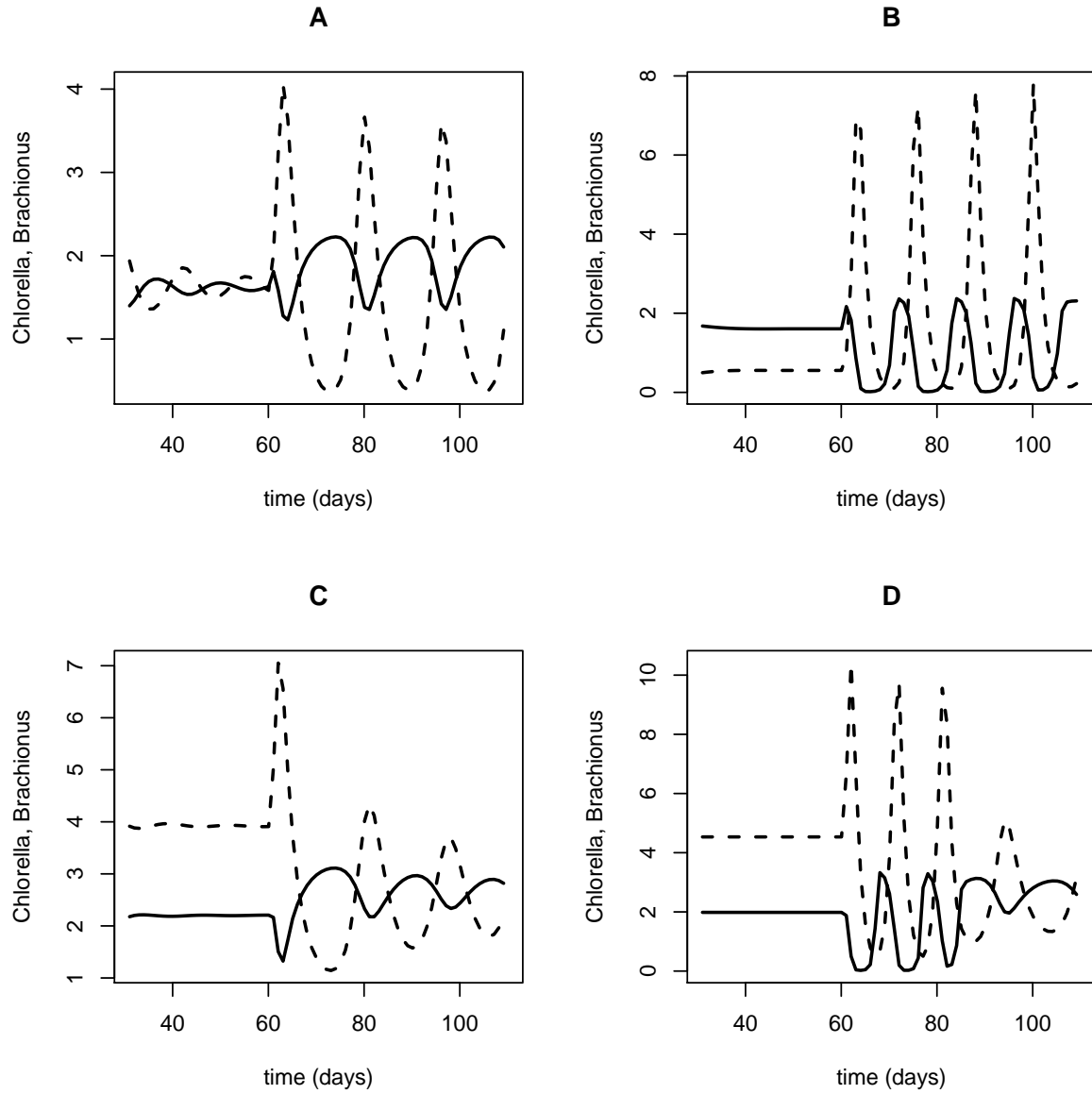


Figure 8: Effects of change in dilution rate on an evolutionarily dynamic system. Panels A, B: for $\alpha_1 < 1$. Evolutionary dynamics are as in Figure 3 D; parameters are as follows: $\alpha_1 = 0.765$, $\alpha_2 = 8.23$, $p_{min} = 0.07$, $\chi_b = 6400$. Panel A: Initial dilution rate $\delta = 1.15$ stepped down to $\delta = 0.7$ at $t = 60$; B, Initial dilution rate $\delta = 1.65$ stepped down to $\delta = 0.7$ at $t = 60$. Panels C, D: for $\alpha_1 > 1$. Evolutionary dynamics are as in Figure 6 B; parameters $\alpha_1 = 1.087$, $\alpha_2 = 9.79$, $p_{min} = 0.12$, $\chi_b = 5419$. Rotifers are shown in dashed line and *Chlorella* in bold line. Panel C, Initial dilution rate $\delta = 1.2$ stepped down to $\delta = 0.7$ at $t = 60$; D, Initial dilution rate $\delta = 1.45$ stepped down to $\delta = 0.7$ at $t = 60$.

6 Discussion

Our analysis of evolutionary dynamics suggests that small, gradual changes in external conditions can precipitate dramatic shifts in community composition or species' densities. This can occur for either qualitative type of tradeoff curve (Figure 1), through two different mechanisms.

For $\alpha_1 < 1$, extreme prey types are favored and an internal ESS cannot exist. Instead, the prey population is dominated either by an endpoint ESS (the minimum or maximum possible food values), or an ESC consisting of the two extreme types. Under a small change in conditions, the evolutionary steady state can jump from one endpoint ESS to another, resulting in a discontinuous change in species abundances (Figure 7AB).

For $\alpha_1 > 1$, an internal ESS may be present at high dilution rates, depending on the shape and cost parameters α_1 and α_2 , and rotifer conversion efficiency χ_b . Where an internal ESS does not exist, the population is dominated either by an endpoint ESS composed of the minimum food value clone present in the system, p_{min} , or an ESC of coexisting types. Simulations indicate that the ESC consists of the two extreme types p_{min}, p_{max} in proportions such that the average food value of the population approximates that of the ESS candidate (which satisfies the first order condition but not the second order condition for evolutionary stability). Because the ESC consists of two very different types, the balance between them is strongly affected by relatively small changes in conditions. As a result, the response of the system (including evolutionary changes in the prey) is very different, not only in magnitude but in direction, from what would be predicted if evolutionary changes in the prey are ignored.

Experiments are in progress to determine the shape of the tradeoff curve in our system. Circumstantial evidence supports a tradeoff curve where extreme types are favored ($\alpha_1 < 1$):

- The best fits of the model to qualitative properties of the experimental data (in particular the transition points between stability and cycles as a function of dilution rate, and properties of the cycles) are obtained with $\alpha_1 < 1$.
- The variability in cycle period (roughly 20-40d) observed in experiments can occur in the model when $\alpha_1 < 1$ (depending on which clones are present), but not for $\alpha_1 > 1$ (Yoshida et al. 2003).

This raises the possibility that a rapid jump from one extreme prey type to another, as predicted by the model, may be experimentally observable in our system.

Our analysis complements recent work by Abrams and Vos (in press) on a general model

for a resource-consumer-predator food chain, with adaptive change in a consumer trait affecting food consumption and mortality rates. Their goal was to predict how perturbations at one trophic level - such as an increase in predator mortality - would propagate through the chain and alter other species' abundances, in the presence of consumer adaptation. The predictions from purely ecological models that ignore consumer adaptation have sometimes been supported, but are also contradicted by numerous experimental studies (Abrams and Vos in press). Abrams and Vos (in press) showed that consumer adaptation broadens the range of theoretically possible responses, and so might explain some cases where purely ecological models failed. For example, without adaptation an incremental increase in consumer mortality in their model always entails an increase in resource abundance and a decrease in predator abundance; with consumer adaptation the resource abundance may decrease and predator density may decrease.

Abrams and Vos (in press) consider a spectrum of models with different assumptions about the composition of the consumer trophic level and the nature of response – e.g., assuming a single phenotypically homogenous consumer species responding behaviorally, or a pair of consumer species changing in relative abundance – and found that predictions about total consumer abundance were robust across a range of models. In our analysis the composition of the consumer trophic level is not assumed, but is one of the predicted outcomes from the clonal selection dynamics. As a result, we can predict how prey evolution can lead to qualitative changes in the genetic composition of the prey population, and how these qualitative changes can lead to abrupt population responses to gradual changes in conditions, as well as the gradual changes predicted by the Abrams-Vos models.

Working with well-characterized model ecological systems (e.g., Mueller and Joshi 2000, Cushing et al. 2002) makes it feasible to study processes that would be far less tractable in the field, and less amenable to rigorous testing of theoretical predictions. Our results lay the groundwork for rigorous tests of the longstanding but still contentious hypothesis that population management must be “evolutionarily enlightened” (Ashley et al. 2003), rather than continuing to take an exclusively ecological perspective (Stockwell et al. 2003).

A Appendix

A.1 $\alpha_1 < 1$

To see that we cannot have an ESC including any interior types, consider a coexisting set κ of two or more genotypes, which has an interior member l and some other member j . By

definition we have $\lambda(p_l|\kappa) = \lambda(p_j|\kappa) = 0$, and as a result of the positive second derivative (18) we conclude that κ must be invisable by some other interior genotype near p_l . Thus, κ as defined cannot be an ESC.

We now analyze the qualitative properties of the invasion exponent functions for $\alpha_1 < 1$. Consider first $\lambda(p_{max}|p)$ for low flow-rate δ (Figure 3A). For a resident type with p near 0 we have $\bar{B} = 0$ (the predators cannot persist) so defense against predation has no value and any clone with higher p can invade, implying that $\lambda(p_{max}|p) > 0$. As the food value p of the resident type increases, the predators can then persist (this bifurcation accounts for the corner in the plot of $\lambda(p_{max}|p)$). We can approximate $\lambda(p_{max}|p) > 0$ for δ small, by inserting the Taylor series expansions of the steady-state values $(\bar{N}, \bar{B}, \bar{C})$ about $\delta = 0$ into (11). This gives

$$\delta^{-1}\lambda(p_{max}|p) = \frac{1}{p} - \theta_1 + O(p) + O(\delta)$$

where $\theta_1 = N_I\chi_c[\chi_b G - (m + \lambda)]/[K_b(m + \lambda)]$. The estimated value of θ_1 from our experimental data, depending on the value of χ_b , is in the range 16.3 – 26.8, causing $\lambda(p_{max}|p)$ to become negative roughly at $p = \theta_1^{-1} \doteq 0.04 - 0.06$. Thus, the qualitative behavior of $\lambda(p_{max}|p)$ at small p is robust to any parameter changes such that $\theta_1 \gg 1$ continues to hold.

Similarly, for $\delta^{-1}\lambda(p|p_{max})$ near $p = 0$ we obtain

$$\delta^{-1}\lambda(p|p_{max}) = \theta_1 \frac{K_c(p_{max})}{K_c(p)} - (\theta_1 - 1)p - 1 + O(\delta).$$

Thus $\lambda(p|p_{max}) > 0$ for p small if $\frac{K_c(p_{max})}{K_c(0)} > 1/\theta_1$, which is true for our estimated parameters (the LHS is at least ≈ 0.25 , the RHS no more than ≈ 0.06). However, as p increases the θ_2 term dominates, and $\lambda(p|p_{max})$ becomes negative, as seen in Figure 3A. As $\delta \rightarrow 0$ both scaled invasion exponents approach limiting shapes similar to the curve shown in bold (Figure 3A).

For low and high flow regimes, as $p \rightarrow 1$ the slopes of both invasion exponents become infinite (Figure 3AB). With some algebra we can show that this feature depends only on the value of α_1 . In the limit as $p \rightarrow p_{max} = 1$, from (12) we have

$$\frac{\partial\lambda(p_{max}|p)}{\partial p} \sim +\text{Constant} \times \frac{\partial K_c}{\partial p}$$

and

$$\frac{\partial\lambda(p|p_{max})}{\partial p} \sim -\text{Constant} \times \frac{\partial K_c}{\partial p}.$$

Since $\frac{\partial K_c}{\partial p} = -\alpha_1\alpha_2(1-p)^{\alpha_1-1}$ and $\alpha_1 < 1$, then $\frac{\partial\lambda(p_{max}|p)}{\partial p} \rightarrow -\infty$ and $\frac{\partial\lambda(p|p_{max})}{\partial p} \rightarrow +\infty$ as $p \rightarrow p_{max}$.

A.2 $\alpha_1 > 1$

Here we derive the properties of the function $g(p)$ defining the second-order condition, that were used in the case $\alpha_1 > 1$. As usual these properties depend on parameter values and our goal is to identify which parameters or parameter combinations control the relevant properties.

(a) $g(p^*)$ is a decreasing function of α_1 for all $\alpha_1 > 0$

Substituting the steady state expressions (8) into (15), we rewrite g as a function of α_1 .

Taking a partial derivative of this expression with respect to α_1 yields

$$\frac{\partial g(p^*)}{\partial \alpha_1} = \frac{K_c(p)'}{2} \left[(3\alpha_1 - 1) - (\alpha_1 - 1) \frac{\gamma + 2N_I}{\sqrt{\gamma^2 + 4N_I K_c(p^*)}} \right] - [\bar{N} + K_{c_{min}} - \alpha_2(1-p)^{\alpha_1}]$$

where γ is defined in equation (9), and $K_c'(p) = \frac{\partial K_c(p)}{\partial \alpha_1} = \alpha_2 \ln(1-p)(1-p)^{\alpha_1}$.

Note that $K_c'(p)$ is negative for any $0 < p < 1$. The expression in the first of the two square brackets is always positive and remains bounded between $\approx 1.4 - 2$ as N_I is either increased from its present value by up to ten times or reduced to zero, and χ_b assumes the range of values we obtained in our optimized parameter sets ($\chi_b = 4000 - 6500$). The expression in the second square bracket has a lower bound of ≈ 4.5 , and is also always positive. We thus have:

$$\frac{\partial g(p^*)}{\partial \alpha_1} \doteq -[\text{“+”}] - [\text{“+”}]$$

and $g(p^*)$ is always a decreasing function of α_1 for any dilution rate δ within our experimental range, and for biologically reasonable choices of the experimental parameter N_I and the fitted parameter χ_b .

(b) $g(p^*)$ is a decreasing function of χ_b

Substituting the steady state expressions (8) into (15), we rewrite g as a function of χ_b .

Taking a partial derivative of this expression with respect to χ_b yields

$$\frac{\partial g(p^*)}{\partial \chi_b} = F(\gamma) = \frac{(\alpha_1 - 1)}{2} \gamma' \left\{ 1 - \frac{\gamma}{\sqrt{\gamma^2 + 4N_I K_c(p^*)}} \right\} \quad (19)$$

where γ is defined in equation (9). $F(\gamma)$ thus has the same sign as γ' , which may be written as follows:

$$\gamma' = \frac{\partial \gamma}{\partial \chi_b} = - \left\{ \frac{\rho_c K_b G(\delta + m + \lambda)}{\delta p [\chi_b G - (\delta + m + \lambda)]^2} \right\}.$$

The expression within the curly brackets is always positive, thus $F(\gamma) < 0$ and thus $g(p)$ is a decreasing function of χ_b for $\alpha_1 > 1$.

(c) $g(p^*)$ is a decreasing function of δ for δ small, and an increasing function of δ when δ is large for $\alpha_1 > 1$

Again substituting the steady state expressions (8) into (15), we can rewrite g as a function of δ . Taking a partial derivative of this expression with respect to δ yields

$$\frac{\partial g}{\partial \delta} = F(\gamma)$$

where $F(\gamma)$ is the expression on the right-hand side of equation (19) and γ is defined in equation (9). As above, $F(\gamma)$ has the same sign as γ' , which may be written as follows:

$$\gamma' = \frac{\partial \gamma}{\partial \delta} = \frac{\rho_C K_b}{p^*} \left\{ \frac{(\delta + m + \lambda)^2 - \chi_b G(m + \lambda)}{[\delta(\chi_B G - m - \lambda) - \delta^2]^2} \right\}$$

This implies that $F(\gamma) < 0$ at low δ , and $F(\gamma) > 0$ at high δ , switching sign at dilution rate

$$\delta_{\text{crit}} = -(m + \lambda) + \sqrt{\chi_b G(m + \lambda)}.$$

References

- [1] Abrams, P. A. (2000). The evolution of predator-prey interactions: theory and evidence. *Annual Review of Ecology and Systematics* 31:79-105.
- [2] Abrams, P. and M. Vos. Adaptation, density dependence, and the responses of trophic level abundances to mortality. *Evolutionary Ecology Research*, *in press*.
- [3] Ashley, M.V., M.F. Willson, O.R.W. Pergams, D.J. O'Dowd, S.M. Gende, and J.S. Brown (2003). Evolutionarily enlightened management. *Biological Conservation* 111: 115-123.
- [4] Cousyn, C., L. De Meester, J.K. Colbourne, L. Brendonck, D. Verschuren, and F. Volckaert (2001). Rapid, local adaptation of zooplankton behavior to changes in predation pressure in the absence of neutral genetic changes. *Proc. Natl. Acad. Sci. USA* 98: 6256-6260.
- [5] Cushing, J. M., R. F. Costantino, B. Dennis, R. A. Desharnais, S. M. Henson (2002). *Chaos in ecology: experimental nonlinear dynamics*. Theoretical Ecology Series Volume I, Academic Press, San Diego.
- [6] Dieckmann, U. (1997). Can adaptive dynamics invade? *Trends in Ecology and Evolution* 12: 128-131.
- [7] Dercole F, J.O. Irisson, and S. Rinaldi (2003). Bifurcation analysis of a prey-predator coevolution model. *SIAM Journal on Applied Mathematics* 63: 1378-1391.
- [8] Ellner S. P. and N. G. Hairston, Jr. (1994). Role of overlapping generations in maintaining genetic variation in a fluctuating environment. *The American Naturalist* (143) 403-417.
- [9] Fussmann G. F., S. P. Ellner, K. W. Shertzer, N. G. Hairston, Jr. (2000). Crossing the Hopf bifurcation in a live predator-prey system. *Science* (290)1358-1360.
- [10] Fussmann, G. F., S.P. Ellner, and N.G. Hairston, Jr. Evolution as a critical component of plankton dynamics. *Proceedings of the Royal Society of London Series B* 270: 1015-1022.
- [11] Grant, P.R. and B.R Grant (2002) Unpredictable evolution in a 30-year study of Darwin's finches. *Science* 296, 707-711.
- [12] Hairston, N.G., W. Lampert, C.E. Cceres, C.L. Holtmeier, L.J. Weider, U. Gaedke, J.M. Fischer, J.A. Fox, J.A. and D. M. Post (1999). Lake ecosystems: Rapid evolution revealed by dormant eggs. *Nature* 401: 446.

- [13] Johnson, M.T.J. and A. Agrawal (2003). The ecological play of predator-prey dynamics in an evolutionary theatre. *Trends in Ecology and Evolution* 18: 549–551.
- [14] Khibnik, A.I. and A.S. Kondrashov (1997). Three mechanisms of Red Queen dynamics. *Proceedings of the Royal Society of London Series B* 264: 1049–1056.
- [15] Le Galliard J.F., R. Ferriere, and U. Dieckmann (2003). The adaptive dynamics of altruism in spatially heterogeneous populations. *Evolution* 57: 1–17.
- [16] Law, R. and D.R. Grey (1989). Evolution of yields from populations with age-specific cropping. *Evolutionary Ecology* 3: 343–359.
- [17] Levin, S.A. and H.C. Muller-Landau (2000). The evolution of dispersal and seed size in plant communities. *Evolutionary Ecology Research* 2: 409–435.
- [18] Marrow, P., U. Dieckmann and R. Law (1996). Evolutionary dynamics of predator-prey systems: An ecological perspective. *Journal of Mathematical Biology* 34: 556–578.
- [19] Morin, P. (1999). *Community Ecology*. Blackwell Science.
- [20] Mueller, L. D. and A. Joshi (2000). *Stability in Model Populations*. Monographs in Population Biology (31), Princeton University Press, Princeton and Oxford.
- [21] Pickett-Heaps, J. D. 1975. *Green Algae: Structure, Reproduction and Evolution in Selected Genera*. Sinauer Associates, Sunderland MA.
- [22] Reznick D.N., F. H. Shaw, F. H. Rodd, R. G. Shaw (1997). Evaluation of the Rate of Evolution in Natural Populations of Guppies (*Poecilia reticulata*). *Science* 275, 1934–1937.
- [23] Reznick, D.N. and C. K. Ghalambor (2001). The population ecology of contemporary adaptations: what empirical studies reveal about the conditions that promote adaptive evolution. *Genetica* 112–113: 188–198.
- [24] Shertzer K. W., S. P. Ellner, G. F. Fussmann, N. G. Hairston, Jr. (2002). Predator–prey cycles in an aquatic microcosm: testing hypotheses of mechanism. *Journal of Animal Ecology* (71) 802–815.
- [25] Sinervo, B. et al. (2000). Density cycles and an offspring quantity and quality game driven by natural selection. *Nature* 406, 985–988.
- [26] Stockwell C.A., A.P. Hendry, and M.T. Kinnison (2003). Contemporary evolution meets conservation biology. *Trends in Ecology and Evolution* 18: 94–101.
- [27] Thompson, J.N. (1998). Rapid evolution as an ecological process. *Trends in Ecology and Evolution* 13: 329–332.

- [28] Yoshida T., L. E. Jones, S. P. Ellner, G. F. Fussmann, N. G. Hairston, Jr. (2003). Rapid evolution drives ecological dynamics in a predator-prey system. *Nature* (424) 303–306.
- [29] Zimmer, C. (2003) Rapid evolution can foil even the best-laid plans. *Science* 300: 895.